Dynamic Polarization of Nuclei by Electron-Nuclear Dipolar Coupling in Crystals*†

O. S. LEIFSON AND C. D. JEFFRIES
Department of Physics, University of California, Berkeley, California
(Received February 2, 1961)

This paper is concerned with a detailed investigation of the dynamic polarization of the protons in $(Ce,La)_2Mg_3(NO_3)_{12}\cdot 24H_2O$ which occurs when one saturates the "forbidden" microwave transitions that simultaneously flip a proton spin and a Ce^{3+} electron spin. The rate equations for the electron and nuclear polarization are solved for (a) a simple ideal model, (b) a model for the case where the forbidden lines are not resolved, and (c) a model taking into account nuclear-spin temperature diffusion. An apparatus for simultaneous observation of proton magnetic resonance and Ce^{3+} paramagnetic resonance at liquid helium temperatures is described. The Ce^{3+} spin-lattice relaxation time T_{1e} is directly measured by a transient method, and it is found that $T_{1e}\propto T^{-14\pm 2}$ for temperatures in the range $1.9°K<T<2.7°K$. In the same crystals, the proton relaxation time T_{1n} is also measured by a transient method and found to be $T_{1n}\propto T^{-7}$ and dependent on the concentration of Ce^{3+} ions. The relative magnitudes of T_{1n} and T_{1e} are best explained by a model intermediate between (a) and (c). At $T\approx 1.5°K$ and a microwave frequency $\nu_e\approx 9.3$ kMc/sec, the proton polarization is observed for a number of different concentrations of Ce^{3+}. The magnitude of the polarization, its dependence on magnetic field and microwave power, and the transient behavior are studied and qualitatively explained. In a crystal containing 1% Ce, the proton polarization is observed to become greater than the thermal equilibrium value by the factor 150, which is about one-quarter of the theoretical ideal. At higher microwave frequencies ($\nu_e\approx 50$ kMc/sec) it should be possible to obtain in this crystal sufficient proton polarization ($\sim 25\%$) to be useful for dynamic nuclear cooling experiments and nuclear targets.

I. INTRODUCTION

THERE have been many modifications and extensions of Overhauser's[1] stimulating proposal that the polarization of nuclei coupled to electrons may be considerably enhanced through certain hyperfine relaxation processes if the electron paramagnetic resonance is saturated. The modification with which we are concerned here is that of strongly inducing, by an applied rf field, forbidden transitions in paramagnetic resonance which simultaneously flip an electron spin **S** and a nuclear spin **I**.[2] (The term "rf" will be used to include microwave frequencies.) This method has been used to orient nuclei in the case where there is a relatively strong coupling of the form $A\mathbf{I}\cdot\mathbf{S}$ between the electron of a paramagnetic ion and the nucleus of the same ion.[3,4] It has also been used in the case of weak dipolar coupling between **I** and **S** in a prototype experiment[5] on a crystal of LiF, where **I** was represented by the spin of Li^6 and **S** by the spin of F^{19}. The subsequent application to electron spins in dipolar coupling with the nuclei of nearby diamagnetic atoms in solids has been widely reported.[6–12] For a general survey of dynamic nuclear orientation we refer to review papers.[13–16]

The electron-nuclear dipolar coupling experiments consist in placing the sample, e.g., a crystal containing the spins **I** and **S**, in a magnetic field H and in a microwave cavity driven at the frequency $\nu_e\sim 10^{10}$ cps. The nuclear magnetic resonance at frequency $\nu_n\sim 10^7$ cps is observed simultaneously by means of an auxiliary coil in the cavity and is used as a measure of the nuclear polarization. When the field is set near the electron spin resonance value H_0, the nuclear polarization is observed to become very small. At the field $H\approx H_0[1+\nu_n/\nu_e]$, corresponding to rf saturation of the forbidden transition which simultaneously flips **I** and **S**, the nuclear polarization is observed to become greater than its thermal equilibrium value by a factor $\sim 10^2$; at $H\approx H_0[1-\nu_n/\nu_e]$, the polarization is similarly enhanced but reversed in sign. One finds at helium temperatures a significant nuclear polarization, of the order of magnitude 10%. The phenomenon is very general; it has been observed in dilute paramagnetic crystals, in free radicals dissolved in plastics, in ir-

* Supported in part by the U. S. Atomic Energy Commission and the Office of Naval Research.
† Some of the material in this paper is taken from the Ph.D. dissertation of O. S. Leifson, University of California, Berkeley, California, July, 1960 (unpublished).
[1] A. Overhauser, Phys. Rev. **89**, 689 (1953); **92**, 411 (1953).
[2] C. D. Jeffries, Phys. Rev. **106**, 164 (1957).
[3] M. Abraham, R. W. Kedzie, and C. D. Jeffries, Phys. Rev. **106**, 165 (1957).
[4] F. M. Pipkin and J. W. Culvahouse, Phys. Rev. **106**, 1102 (1957).
[5] A. Abragam and W. G. Proctor, Compt. rend. **246**, 2253 (1958).
[6] A. Abragam, J. Combrisson, and I. Solomon, Compt. rend. **247**, 2237 (1958).
[7] M. Abraham, M. A. H. McCausland, and F. N. H. Robinson, Phys. Rev. Letters **2**, 449 (1959).
[8] M. Borghini and A. Abragam, Compt. rend. **248**, 1803 (1959).
[9] J. A. Cowan, W. R. Schafer, and R. C. Spence, Phys. Rev. Letters **3**, 13 (1959).
[10] O. S. Leifson, P. L. Scott, and C. D. Jeffries, Bull. Am. Phys. Soc. **4**, 453 (1959); P. L. Scott, O. S. Leifson, and C. D. Jeffries, Bull. Am. Phys. Soc. **4**, 453 (1959).
[11] J. Combrisson and I. Solomon, J. Phys. radium **20**, 683 (1959).
[12] Chester Hwang and T. M. Sanders, Jr., *Proceedings of the 7th International Conference on Low-Temperature Physics* (University of Toronto Press, Toronto, 1960), p. 98.
[13] E. Ambler, *Progress in Cryogenics* (Heywood and Company, Ltd., London; and Academic Press, Inc., New York, 1960), Vol. II.
[14] C. D. Jeffries, *Progress in Cryogenics* (Heywood and Company, Ltd., London; and Academic Press, Inc., New York, 1961), Vol. III.
[15] C. D. Jeffries, Phys. Rev. **117**, 1056 (1960).
[16] G. R. Khutsishvili, Uspekhi Fizicheskikh Nauk **71**, 9 (1960). [Translation: Soviet Phys.—Uspekhi **3**, 285 (1960)].

radiated crystals and plastics, and in P-doped silicon. The phenomenon was discovered[17] in liquids prior to the work in solids. In fact, even earlier, dynamic nuclear polarization by dipolar coupling in nuclear double-resonance experiments had been discussed by Bloembergen and Sorokin,[18] who are probably the originators of the method.

The present paper is a detailed discussion of this method of dynamic nuclear polarization and, in particular, its application to the polarization of protons in the double nitrate crystal $(La,Ce)_2Mg_3(NO_3)_{12}\cdot 24H_2O$ in which the paramagnetic Ce^{3+} concentration is a small fraction of the diamagnetic La^{3+} concentration. This well-known crystal is particularly appropriate for study since $I=\frac{1}{2}$ for protons and $S=\frac{1}{2}$ for Ce^{3+} ions; the nuclear spin of Ce is zero and no additional hfs lines complicate the analysis. Polarization in this crystal has also been studied by others.[7,19] Some of the results in the present paper have already been briefly reported.[14,20]

In Sec. II A we take a simplified phenomenological model and calculate the nuclear polarization obtainable when the forbidden lines are well resolved; in Sec. II B we extend this to the case of unresolved lines; in Sec. II C we consider briefly the effects of spatial diffusion of nuclear polarization. Although the treatment has some generality we usually take numerical values appropriate to the double nitrate crystal. In Sec. III, the apparatus is described and in Sec. IV we give our experimental results and interpretation.

II. THEORY

We consider a magnetically dilute solid containing N electron spins and n nuclear spins in a magnetic field $\mathbf{H}$ at a low temperature. We assume that either the electron g-tensor is isotropic, or else that a principal axis is parallel to $\mathbf{H}$. Let $\mathbf{S}_k$ be the kth electron spin and $\mathbf{I}_i$ the ith nuclear spin. The spin Hamiltonian for the entire sample will be taken to be

$$\mathcal{H}=g\beta\sum_k \mathbf{H}\cdot\mathbf{S}_k-g_n\beta\sum_i \mathbf{H}\cdot\mathbf{I}_i+\sum_{i,k} V_{ik}+\sum_{i>j} U_{ij}, \quad (1)$$

where β is the Bohr magneton and g, g_n are the electron, nuclear g factors, respectively. The terms represent the electron Zeeman, nuclear Zeeman, electron-nuclear, and nuclear-nuclear interactions, respectively. We neglect electron-electron interactions because we assume the sample is dilute in electron spins: $N\ll n$. We neglect nuclear quadrupole interactions because we are primarily interested in the case $I=\frac{1}{2}$. The third term may be written as the sum of a contact type of interaction and a dipole-dipole interaction,

$$V_{ik}=\mathbf{I}_i\cdot A_{ik}\cdot\mathbf{S}_k-\frac{gg_n\beta^2}{r_{ik}^3}\left[\mathbf{I}_i\cdot\mathbf{S}_k-\frac{3(\mathbf{I}_i\cdot\mathbf{r}_{ik})(\mathbf{S}_k\cdot\mathbf{r}_{ik})}{r_{ik}^2}\right], \quad (2)$$

where A_{ik} is a tensor and $\mathbf{r}_{ik}$ is the displacement vector between $\mathbf{I}_i$ and $\mathbf{S}_k$. The term U_{ij} is the dipole-dipole interaction between $\mathbf{I}_i$ and $\mathbf{I}_j$:

$$U_{ij}=\frac{g_n^2\beta^2}{r_{ij}^3}\left[\mathbf{I}_i\cdot\mathbf{I}_j-\frac{3(\mathbf{I}_i\cdot\mathbf{r}_{ij})(\mathbf{I}_j\cdot\mathbf{r}_{ij})}{r_{ij}^2}\right]. \quad (3)$$

Since the electron spins and the nuclear spins are strongly coupled to the $\mathbf{H}$ field and only weakly coupled together through the third term, it is convenient to decompose the system into two sub-systems, the electron (spin) system and the nuclear (spin) system. In zero order, the electron system [first term of Eq. (1)] is represented by the phenomenological spin Hamiltonian $\mathcal{H}=g\beta\mathbf{H}\cdot\mathbf{S}$ and has a magnetic resonance frequency $\nu_e=g\beta H/h$, corresponding to flipping an electron spin: $S_z\rightarrow S_z\pm 1$. Likewise the nuclear system [second term in Eq. (1)] has a magnetic resonance frequency $\nu_n=g_n\beta H/h$ corresponding to flipping a nuclear spin: $I_z\rightarrow I_z\pm 1$. Now the fourth term in Eq. (1) will add a Van Vleck linewidth[21] to the nuclear resonance line and also perhaps a structure.[22] It will also provide a spatial diffusion of nuclear spin temperature through mutual spin flips of neighboring nuclei. Finally, we consider the perturbing effects of the third term of Eq. (1). If V_{ik} is expanded it will contain operator products of the form $(I_x\pm iI_y)(S_z)$ which admix the zero-order states and allow for additional ("forbidden") transitions of the type I_z, $S_z\rightarrow I_z\pm 1$, $S_z\pm 1$ and I_z, $S_z\rightarrow I_z\pm 1$, $S_z\mp 1$. These are sometimes observable[23,24] and appear as a satellite structure on the electron resonance line. The V_{ik} term will also provide a Van Vleck width to the electron resonance line and may add additional structure[25] to the nuclear resonance line, since different nuclear sites may experience different local fields from the electron.

A. Simple Model

For simplicity, we now neglect any structure on the nuclear resonance line and assume that the forbidden lines of the electron resonance are completely resolved; we furthermore neglect spin temperature diffusion. The two loosely coupled systems are represented by the energy level diagram of Fig. 1 for $S=\frac{1}{2}$ and $I=\frac{1}{2}$. We

[17] E. Erb, J. L. Motchane, and J. Uebersfeld, Compt. rend. **246**, 2121, 3050 (1958).
[18] N. Bloembergen and P. P. Sorokin, Phys. Rev. **110**, 865 (1958).
[19] M. A. H. McClausland, thesis, Oriel College, Oxford, 1959 (unpublished).
[20] C. D. Jeffries, Bull. Am. Phys. Soc. **5**, 495 (1960), paper E4; O. S. Leifson and C. D. Jeffries, Bull. Am. Phys. Soc. **6**, 225 (1961), paper A7.
[21] J. H. Van Vleck, Phys. Rev. **74**, 1168 (1948).
[22] G. E. Pake, J. Chem. Phys. **16**, 327 (1948).
[23] H. Zeldes and R. Livingston, Phys. Rev. **96**, 1702 (1954); G. J. Trammel, H. Zeldes, and R. Livingston, *ibid.* **110**, 630 (1958).
[24] J. M. Baker, W. Hayes, and M. C. M. O'Brien, Proc. Roy. Soc. (London) **A254**, 273 (1960).
[25] N. Bloembergen, Physica **16**, 95 (1950).

take g to be positive, as for a free electron spin, let N_1 be the population of the upper electron state $\langle S_z\rangle = M = +\frac{1}{2}$, and let $N_2 = N - N_1$ be the population of the lower state $M = -\frac{1}{2}$. Similarly, we take g_n positive, as for a proton, and let n_1 be population of the upper nuclear spin state $\langle I_z\rangle = m = -\frac{1}{2}$, etc. We follow Abragam's treatment[26] here. Assume that the lattice vibrations provide a thermal reservoir at a temperature T and represent their influence by a random time-dependent perturbation ${}_T\mathcal{H}(t)$ on the spin Hamiltonian $\mathcal{H}$, which induces the relaxation transitions of the system. The dominant process is the electron spin-lattice interaction ${}_T\mathcal{H}_1 = g\beta\mathbf{H}'(t)\cdot\mathbf{S}$, which provides the usual paramagnetic relaxation transitions $S_z \rightarrow S_z \pm 1$ at a rate w_1/sec, say. The direct (Waller) interaction of the nuclear spins with the lattice is negligible and their chief relaxation in crystals at low temperatures is through electron spins.[27,28] Figure 2 represents the composite energy-level diagram of a typical pair $\mathbf{I}_i$, $\mathbf{S}_k$; we assume that the first term in V_{ik} is negligible. The zero-order wave functions $|M,m\rangle$ become slightly admixed by the static dipolar term. Then the perturbation ${}_T\mathcal{H}_1$ will provide the relaxation σw_1 in Fig. 2, where[26]

$$\sigma = (9/4)(g\beta/Hr^3)^2 \sin^2\theta \cos^2\theta. \quad (4)$$

Here, r is the distance between $\mathbf{I}_i$ and $\mathbf{S}_k$ and θ is the angle between r and H, and it has been assumed that $\nu_n \gg w_1$, which is a good approximation at helium temperatures. Actually, the dipolar admixtures are not static and there will be the additional relaxation transitions Θw_1 shown in Fig. 2, whose rate will probably not exceed σw_1. Both represent relaxation of the nuclear spins through the electron, the one involving simultaneous spin flips, the other only nuclear spin flips. There is also the probability that the sample may contain other, undesirable, electron spins S', e.g., those of dissolved oxygen gas, which give rise to an average nuclear relaxation rate φw_1, say, in addition to σw_1 and Θw_1. Or, alternatively, φw_1 may represent the direct nuclear lattice relaxation in cases where it is unusually large, e.g., in solid H_2 because of molecular rotation. For $H \approx 3600$ oe and $g \approx 1.83$, typical for our experiments, Eq. (4) yields $\sigma \approx 6.6r^{-6}$, if r is measured in angstroms and the spatial average $\cos^2\theta \sin^2\theta = 2/15$ is taken.

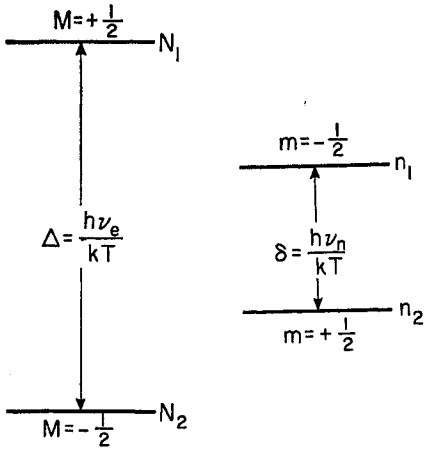

FIG. 1. Energy level diagram and populations for a system of nuclear spins $I=\frac{1}{2}$ loosely coupled to electron spins $S=\frac{1}{2}$.

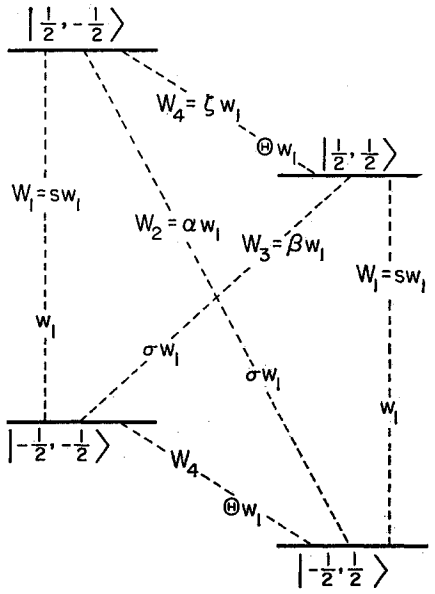

FIG. 2. Energy level diagram and transitions of a nuclear spin $I=\frac{1}{2}$ in dipolar coupling with an electron spin $S=\frac{1}{2}$. The states are labeled by their zero-order functions $|M,m\rangle$.

An applied rf field $2H_1 \cos 2\pi\nu_e t$ perpendicular to $\mathbf{H}$ will induce these transitions[29] in the system of Fig. 2 with the average rates

$$W_1(\tfrac{1}{2}, \pm\tfrac{1}{2} \leftrightarrow -\tfrac{1}{2}, \pm\tfrac{1}{2}) \equiv sw_1 = \tfrac{1}{2}\pi\gamma H_1^2 G(H-H_0) \text{ sec}^{-1}, \quad (5)$$

$$W_2(\tfrac{1}{2}, -\tfrac{1}{2} \leftrightarrow -\tfrac{1}{2}, \tfrac{1}{2}) \equiv \alpha w_1 = \tfrac{1}{2}\rho\pi\gamma H_1^2 G(H-H_-) \text{ sec}^{-1}, \quad (6)$$

$$W_3(\tfrac{1}{2}, \tfrac{1}{2} \leftrightarrow -\tfrac{1}{2}, -\tfrac{1}{2}) \equiv \beta w_1 = \tfrac{1}{2}\rho\pi\gamma H_1^2 G(H-H_+) \text{ sec}^{-1}, \quad (7)$$

where $\gamma = g\beta/\hbar$, $\rho = \frac{3}{10}(g\beta/r^3H)^2 \sim \sigma$, and G is the electron resonance line shape function, so normalized that $\int_0^\infty G(H)dH = 1$ and $G_{\max} \equiv \gamma T_{2e}/\pi$. W_1 corresponds to the usual allowed electron line at H_0; and W_2 and W_3 are the forbidden lines at $H_- = H_0(1-g_n/g)$ and $H_+ = H_0(1+g_n/g)$.

A perpendicular rf field $2H_{1n} \cos 2\pi\nu_n t$ will induce pure nuclear transitions at the rate

$$W_4(\pm\tfrac{1}{2}, -\tfrac{1}{2} \leftrightarrow \pm\tfrac{1}{2}, \tfrac{1}{2}) \equiv \zeta w_1 = \tfrac{1}{2}\pi\gamma_n H_{1n}^2 G_n(H-H_{0n}) \text{ sec}^{-1}, \quad (8)$$

[26] A. Abragam, Phys. Rev. **98**, 1729 (1955).
[27] N. Bloembergen, Physica **15**, 386 (1949).
[28] J. Hatton and B. V. Rollin, Proc. Roy. Soc. (London) **A199**, 222 (1949).
[29] See, e.g., reference 15, Eqs. (21), (47c), and (47d).

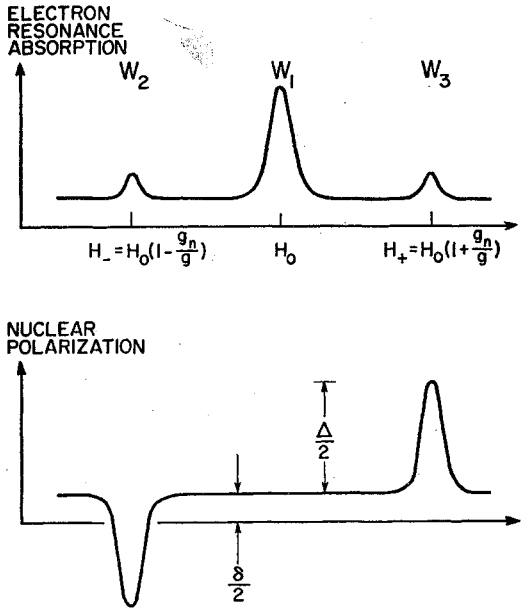

FIG. 3. Idealized electron magnetic resonance spectrum showing the central W_1 transition and the two "forbidden" transitions, W_2 and W_3. When the latter are strongly induced, an enhanced nuclear polarization results.

where $\gamma_n=g_n\beta/\hbar$, G_n is the nuclear resonance line shape function, and $H_{0n}=h\nu_n/g_n\beta$. These transitions are used in monitoring the nuclear polarization.

Still considering the typical pair of Fig. 2, we see that if Θ, $\sigma\ll 1$, and if we strongly induce only transition W_3, then the relative population of the $|\frac{1}{2},\frac{1}{2}\rangle$ and $|-\frac{1}{2},-\frac{1}{2}\rangle$ states become equal, say, to unity. However the relaxation rate w_1 is sufficient to maintain the relative population of the $|-\frac{1}{2},\frac{1}{2}\rangle$ state at e^{Δ} and that of the $|\frac{1}{2},-\frac{1}{2}\rangle$ state at $e^{-\Delta}$, where $\Delta\equiv h\nu_e/kT$. Thus the dynamic nuclear polarization becomes, ideally,

$$p\equiv\frac{n(m=+\frac{1}{2})-n(m=+\frac{1}{2})}{n(m=+\frac{1}{2})+n(m=-\frac{1}{2})}=\frac{\sinh\Delta}{1+\cosh\Delta}\approx\frac{\Delta}{2}, \quad (9)$$

which is $\Delta/\delta=g/g_n$ times larger than the thermal equilibrium value $p_0=h\nu_n/2kT$. Similarly inducing W_2 yields $p\approx-\Delta/2$; Fig. 3 illustrates the over-all effect.

Turning now to the question of the nuclear polarization of the whole sample, we note that each electron is in dipolar coupling with very many nuclei, some being rather far away. The diffusion of nuclear polarization becomes important since the rates σw_1, αw_1, $\cdots$, being proportional to r^{-6}, become very small. The eventual effect of diffusion is to bring the system into self-equilibrium, and we approximate this by a simple hypothetical model in which the n nuclear spins are assumed to be all alike (i.e., have the same average values of σ, α, $\cdots$) and share equally the N electrons which are the source of their polarization and, partially, their relaxation. Thus we consider again Fig. 1 as the diagram for the entire sample and write the rate equations for the populations under the simultaneous action of the rf transition rates sw_1, αw_1, βw_1, and ζw_1 and the relaxation rates w_1, Θw_1, σw_1, and φw_1:

$$\begin{aligned}-dn_2/dt=dn_1/dt=&(n_2-n_1)\zeta w_1-n_1\varphi w_1(1+\tfrac{1}{2}\delta)+n_2\varphi w_1(1-\tfrac{1}{2}\delta)\\&-n_1(N/n)(N_1/N)[\alpha+\Theta(1+\tfrac{1}{2}\delta)+\sigma(1+\tfrac{1}{2}\Delta+\tfrac{1}{2}\delta)]w_1-n_1(N/n)(N_2/N)[\beta+\Theta(1+\tfrac{1}{2}\delta)+\sigma(1-\tfrac{1}{2}\Delta+\tfrac{1}{2}\delta)]w_1\\&+n_2(N/n)(N_1/N)[\beta+\Theta(1-\tfrac{1}{2}\delta)+\sigma(1+\tfrac{1}{2}\Delta-\tfrac{1}{2}\delta)]w_1+n_2(N/n)(N_2/N)[\alpha+\Theta(1-\tfrac{1}{2}\delta)+\sigma(1-\tfrac{1}{2}\Delta-\tfrac{1}{2}\delta)]w_1. \quad (10)\end{aligned}$$

The first term is due to the rf transition ζw_1. The next two terms represent the contribution to $\dot{n}_1$ due to the extraneous relaxation φw_1; since these are thermal processes, the rates are weighted by suitable Boltzmann factors (in first order) so that the correct thermal equilibrium populations will be attained. The remaining terms represent the contribution to $\dot{n}_1$ due to the dipolar coupling; the factor (N/n) is approximately the fraction of the time that a given nuclear spin may be undergoing mutual spin flips with an electron, since $n\gg N$.

A similar equation may be written for the electron population, noting that electrons are almost always in coupling with some nucleus and undergoing flips.

$$\begin{aligned}-dN_2/dt=dN_1/dt=&-N_1(n_1/n)[s+\alpha+1+\tfrac{1}{2}\Delta+\sigma(1+\tfrac{1}{2}\Delta+\tfrac{1}{2}\delta)]w_1-N_1(n_2/n)[s+\beta+1+\tfrac{1}{2}\Delta+\sigma(1+\tfrac{1}{2}\Delta-\tfrac{1}{2}\delta)]w_1\\&+N_2(n_2/n)[s+\alpha+1-\tfrac{1}{2}\Delta+\sigma(1-\tfrac{1}{2}\Delta-\tfrac{1}{2}\delta)]w_1+N_2(n_1/n)[s+\beta+1-\tfrac{1}{2}\Delta+\sigma(1-\tfrac{1}{2}\Delta+\tfrac{1}{2}\delta)]w_1. \quad (11)\end{aligned}$$

By introducing the nuclear polarization $p=(n_2-n_1)/(n_2+n_1)$, its thermal equilibrium value $p_0\cong\frac{1}{2}\delta$, the electron polarization $P=(N_1-N_2)/(N_1+N_2)$ and its thermal equilibrium value $P_0\cong-\frac{1}{2}\Delta$, we rewrite these equations as

$$\begin{aligned}dp/dt=&-2w_1[\varphi+(N/n)(\Theta+\sigma)](p-p_0)-2w_1\zeta p\\&-w_1(\alpha N/n)(p-P)-w_1(\beta N/n)(p+P), \quad (12)\end{aligned}$$

$$\begin{aligned}dP/dt=&-2w_1(1+\sigma)(P-P_0)-2w_1sP\\&-w_1\alpha(P-p)-w_1\beta(P+p). \quad (13)\end{aligned}$$

These basic equations exhibit the usual transient behavior of spin systems. For example, if $\zeta\approx 0$, $\alpha=0$, $\beta=0$ in Eq. (12), then $p\rightarrow p_0$ exponentially in a characteristic time

$$T_{1n}\equiv\{2w_1[\varphi+(N/n)(\Theta+\sigma)]\}^{-1}, \quad (14)$$

which we define as the nuclear relaxation time of the sample; it may be directly measured by observing the transient decay of the nuclear resonance signal for ζ sufficiently small. Likewise if $s\approx 0$, $\alpha=0$, $\beta=0$ in Eq. (13), then $P\rightarrow P_0$ in a characteristic time

$$T_{1e}\equiv[2w_1(1+\sigma)]^{-1}, \tag{15}$$

which we define as the electron relaxation time of the sample, observed by the transient decay of the electron resonance signal. If $\alpha\neq 0$ or $\beta\neq 0$, then the equations become coupled; p and P each display two characteristic response times.[30]

In the steady state the nuclear polarization becomes

$$p\approx\frac{\Delta(\alpha-\beta)(1+\sigma)}{(\alpha-\beta)^2-[2(1+\sigma)f+\alpha+\beta+2\zeta n/N][2(1+\sigma)+2s+\alpha+\beta]}, \tag{16a}$$

where we have neglected terms of order $\delta\ll\Delta$, and introduced the parameter

$$f\equiv nT_{1e}/NT_{1n}. \tag{16b}$$

Under the same conditions the electron polarization becomes

$$P\approx\frac{\Delta(1+\sigma)[2(1+\sigma)f+\alpha+\beta+2\zeta n/N]}{(\alpha-\beta)^2-[2(1+\sigma)f+\alpha+\beta+2\zeta n/N][2(1+\sigma)+2s+\alpha+\beta]}. \tag{16c}$$

If we, for example, induce only the forbidden transition W_3 so that $\alpha=0$, $s=0$, $\zeta=0$, $\beta\neq 0$, then, since $\sigma\ll 1$, the steady-state polarizations become

$$P_{ss}\approx-\tfrac{1}{2}\Delta\{(2f+\beta)/[2f+\beta(1+f)]\}, \tag{17a}$$

$$p_{ss}\approx\tfrac{1}{2}\Delta\{\beta/[2f+\beta(1+f)]\}. \tag{17b}$$

The latter becomes

$$p_{\rm sat}=\tfrac{1}{2}\Delta(1+f)^{-1}, \tag{17c}$$

in the limit $\beta\gg 2f/(1+f)$, i.e., for complete saturation of the forbidden transition. This dynamic polarization is less than the ideal value by the factor $(1+f)^{-1}$ and thus f is seen to be a "leakage" factor which is a measure of the extraneous relaxation. From Eqs. (14) and (15), $f\approx\Theta+\sigma+n\varphi/N$ and in the ideal case $\varphi\rightarrow 0$, so that $f\approx\Theta+\sigma\sim\sigma\ll 1$. On the other hand, if the spins S are very dilute, then $f\approx n\varphi/N\gg 1$, thus considerably reducing the maximum obtainable polarization. In other words, it is essential for the full effect that each electron spin mutually flip a total of n/N nuclear spins via a forbidden rf transition in a time less than T_{1n}. To do this, the electrons must have a relaxation time $T_{1e}<NT_{1n}/n$, otherwise there will be a bottleneck in the polarization process.

The saturation behavior of p_{ss} is also an indication of the value of f. Half the maximum polarization, $\frac{1}{2}p_{\rm sat}$, will be obtained for an rf field H_1 given by

$$(\gamma H_1)_{\frac{1}{2}}^2=2f/[\rho T_{1e}T_{2e}(1+f)], \tag{18}$$

since at the line center of W_3, $\beta=\rho T_{1e}T_{2e}(\gamma H_1)^2$. In favorable cases $f\approx\sigma\approx\rho$ and then $(\gamma H_1)_{\frac{1}{2}}^2\approx 2(T_{1e}T_{2e})^{-1}$, which is the same condition to half-saturate the main electron resonance line W_1. In unfavorable cases $f\gg 1$, and $(\gamma H_1)_{\frac{1}{2}}^2\approx 2(\rho T_{1e}T_{2e})^{-1}$, requiring several hundred times more microwave power.

It is convenient to define the enhancement E of the nuclear polarization $E=p_{ss}/p_0$, with an ideal value $E_i=g/g_n$ and a maximum value from Eq. (17c), $E_{\rm sat}=E_i(1+f)^{-1}$. Since T_{1e} and T_{1n} do not necessarily have the same temperature dependence, then f and hence $E_{\rm sat}$ may be a function of temperature. In fact, if T_{1e} increases faster than T_{1n} with decreasing temperature, then $E_{\rm sat}$ may be actually reduced at lower temperatures. Of course at the higher temperatures it becomes difficult to saturate the transitions because of rf power limitations, and E may have a maximum at some optimum temperature.

The general solutions of Eqs. (12) and (13) show the transient build-up to the steady-state values. If only the transition W_3 is excited, then the approximate solutions are

$$p(t)=p_{ss}+[N\beta/n(2+\beta)]C\exp(-t/\tau_1)+D\exp(-t/\tau_2), \tag{19a}$$

$$P(t)=P_{ss}+C\exp(-t/\tau_1)-[\beta/(2+\beta)]D\exp(-t/\tau_2), \tag{19b}$$

where

$$\tau_1=T_{1e}[2/(2+\beta)],$$
$$\tau_2=T_{1n}\{1-(\beta/[2f+\beta(1+f)])\}, \tag{19c}$$

and C and D are constants to be determined by the initial conditions. For example, if $p(0)=p_0\approx 0$ and $P(0)=P_0$ and W_3 is turned on at $t=0$, then

$$p(t)\approx p_{ss}[1-\exp(-t/\tau_2)]. \tag{20a}$$

Thus p exponentially approaches its steady value in a characteristic time τ_2 which is approximately T_{1n} for low rf powers; for saturating powers $\tau_2\approx T_{1n}f(1+f)^{-1}$. Similarly, the electron polarization:

$$P(t)=P_{ss}+P_0\beta(2+\beta)^{-1}\exp(-t/\tau_1)-P_0\beta^2\{[2f+\beta(1+f)](2+\beta)\}^{-1}\exp(-t/\tau_2). \tag{20b}$$

[30] See, for example, I. Solomon, Phys. Rev. **99**, 559 (1955) and R. T. Schumacher, *ibid.* **112**, 837 (1958).

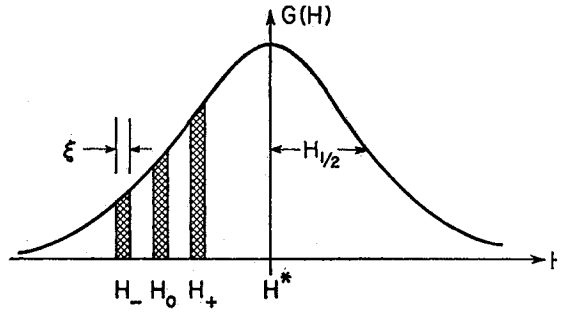

FIG. 4. Schematic diagram of an inhomogeneously broadened electron resonance line composed of rectangular packets.

This shows that P drops from P_0 to a value lower than P_{ss} with a short time constant τ_1 and then increases to P_{ss} with the longer time constant τ_2.

In electron-nuclear double-resonance (ENDOR[31]) experiments, one usually observes the change in intensity of the main electron resonance line which occurs when a nuclear transition is saturated. A similar experiment may be performed on the system under consideration. Suppose that forbidden transition W_3 is strongly saturated and that the polarizations are given by Eqs. (17a) and (17b). If transition W_4 is strongly saturated so that $\zeta n/N \gg f$, β, then $p \to 0$ and $P \to 2(2+\beta)^{-1}P_0$ in a short time, of order $(\zeta n/N)^{-1}$ sec. This change in P will give rise to the fractional change in intensity I_1 of the allowed line

$$\Delta I_1/I_1=\beta^2/[(2f+\beta)(2+\beta)], \tag{21}$$

which approaches unity in the limit $\beta \gg 2$, f. If W_4 is turned off, Eq. (19b) shows that P will return to P_{ss} in a characteristic time τ_2 as the nuclei become polarized again. This behavior has been observed here (see Sec. IV C) and in other crystals.[32,33]

B. Unresolved Spectra

In Sec. II A we have assumed that the electron resonance linewidth is very small compared to $H_0 g_n/g$, as in Fig. 3, so that transitions W_1, W_2, or W_3 may be separately excited at will. This is not the usual case, however, and we must consider the possibility that all transitions may be partially induced, even though we attempt to induce only one of them. First consider the case of a completely inhomogeneously broadened line,[34] shown schematically in Fig. 4, where G(H) is the normalized line shape. The line, of half-width $H_{\frac{1}{2}}$, is imagined to be a superposition of a large number of narrow rectangular packets of width $\xi \ll H_{\frac{1}{2}}$, each thermally isolated from the others. For a constant applied frequency $\nu_e=g\beta H^*/h$ and a variable field H_0, a fraction $\xi G(H_-)$ of the spins will have their W_3 transitions saturated, giving a partial polarization $p_+=p_{ss}\xi G(H_-)$. Similarly a fraction $\xi G(H_+)$ will give $p_-=-p_{ss}\xi G(H_+)$, and the net enhancement will be

$$E(H_0)=\frac{p_++p_-}{p_0}=-\frac{2\xi H_0\beta}{2f+\beta(1+f)}\left(\frac{dG}{dH}\right)_{H_0}, \tag{22}$$

which is considerably reduced and is proportional to the derivative of the electron resonance line shape and independent of g_n. Such a case has been observed.[7,19] The width $\xi \sim (H_1^2+H_{\mathrm{mod}}^2+H_i^2)^{\frac{1}{2}}$, where H_{mod} is the modulation field and H_i the intrinsic packet width.

These simple considerations become invalid when $\xi \approx H_0 g_n/g$ and we next consider the case where $H_i \gg H_0 g_n/g$, i.e., the completely homogeneously broadened line. All spins are simultaneously subject to rf fields inducing the transitions W_1, W_2, and W_3. At very high power levels the populations all tend to become equal in Fig. 2 and the nuclear polarization will be negligible. However, at intermediate levels[35] it is possible to preferentially saturate W_2 or W_3 in the wings of the line, and a differential effect results which is readily calculated from Eq. (16a). Taking $\sigma \ll 1$, $s=cG_0$, $\alpha=\rho cG_-$, and $\beta=\rho cG_+$ where $c=\pi\gamma H_1^2 T_{1e}$ and $G_0=G(H-H_0)$, etc., we find, approximately,

$$p \approx \tfrac{1}{2}\Delta \frac{c(G_+-G_-)}{2f\rho^{-1}+c[2f\rho^{-1}G_0+(1+f)(G_++G_-)]+c^2G_0(G_++G_-)}. \tag{23}$$

To illustrate this behavior we assume a Lorentz lineshape

$$G_0=\{(\pi H_{\frac{1}{2}})[1+(H-H_0)^2/H_{\frac{1}{2}}^2]\}^{-1},$$

and the ideal case $f \approx \sigma \approx \rho \ll 1$, and take the half-width $H_{\frac{1}{2}}=H_0 g_n/g$. The calculated polarization is shown in Fig. 5 as a function of H for several values of the saturation parameter

$$s_0=(\gamma H_1)^2 T_{1e} T_{2e}.$$

For $s_0=0.1$ the polarization is peaked near the field H_+ for the W_3 transition; the optimum polarization $p \approx 0.22(\Delta/2)$ is obtained for $s_0 \approx 3$. For still larger values of s_0, the polarization is reduced and is peaked about a field far from H_+. Behavior qualitatively like this has been observed in the double nitrate crystals (see Sec. IV C), and also in Cu^{++}-doped Tutton salts[10] and in irradiated plastics.

Most electron resonance lines represent an intermediate case between the two extreme cases just

[31] G. Feher, Phys. Rev. **103**, 83 (1956).
[32] R. W. Terhune, J. Lambe, G. Makhov, and L. G. Cross, Phys. Rev. Letters **4**, 234 (1960).
[33] J. Axe, H. J. Stapleton, and C. D. Jeffries, Phys. Rev. **121**, 1630 (1961).
[34] A. M. Portis, Phys. Rev. **91**, 1071 (1953).
[35] J. L. Motchane and J. Uebersfeld, J. phys. radium **21**, 194 (1960).

considered, and a proper treatment must include the effects of cross relaxation.[36]

C. Diffusion Effects

In Sec. II A we naively assumed that somehow an electron interacts with n/N nuclei on the average. For very dilute samples this is far from the actual situation, which is more like this: A nuclear spin which is a nearest neighbor to a paramagnetic ion may be flipped by a relaxation transition σw_1, $\cdots$, or by an rf transition W_2, $\cdots$. This nucleus may then engage in a mutual spin flip with a neighboring nucleus with a rather high transition probability, since energy is very nearly conserved. The process is repeated and the spin temperature of the nuclei nearest the ion diffuses out to nuclei further away. This process was invoked[27,28] some time ago to explain the observed nuclear relaxation times in very dilute crystals at low temperatures.

Diffusion effects are treated approximately by assuming that the polarization $p=p(\mathbf{r},t)$ is a continuous space variable and adding a term $\nabla^2 p$ to the rate equations. In the absence of microwave fields ($\alpha=0$, $\beta=0$, $s=0$) and extraneous nuclear relaxation ($\varphi=0$), Eq. (12) may be rewritten in the form of Bloembergen's diffusion equation,[27]

$$\partial p/\partial t=-C\sum_k|\mathbf{r}-\mathbf{r}_k|^{-6}(p-p_0)-2w_1\zeta p+D\nabla^2 p, \quad (24)$$

where the diffusion constant $D=aW^2$; a=lattice constant; $W\approx(30T_{2n})^{-1}$=transition probability for nearest nuclear neighbors to undergo mutual flip; T_{2n}=transverse nuclear relaxation time; $C=3(g\beta)^2/10H^2T_{1e}$; and $|\mathbf{r}-\mathbf{r}_k|$ is the distance between the nuclear spin at $\mathbf{r}$ and the electron spin at $\mathbf{r}_k$. The summation is over all the electron spins S in the sample. For a proton inverse linewidth $2T_{2n}\approx(50\text{ kc/sec})^{-1}$ and $a\approx 3$ A, we estimate $D\approx 3\times10^{-12}$ cm^2 sec^{-1} for the double nitrate crystal.

Approximate solutions to Eq. (24) have been given[37,38] and involve a summation over k and an integration over $\mathbf{r}$. The result is that the space average nuclear polarization $\bar{p}$ obeys the equation

$$\bar{p}(t)=p_0\frac{1-\exp[(-2w_1\zeta-T_{1n}^{-1})t]}{1+2w_1\zeta T_{1n}}, \quad (25)$$

when $p(0)=p_0$ and $W_4=w_1\zeta$ is turned on at $t=0$. The nuclear resonance signal displays in the limit $W_4\ll T_{1n}^{-1}$ a unique relaxation rate

$$T_{1n}^{-1}=8.5n_0C^{\frac{1}{2}}D^{\frac{3}{4}}\propto H^{-\frac{1}{2}}T_{1e}^{-\frac{1}{2}}, \quad (26)$$

where n_0=number of paramagnetic ions per cm^3. This is to be contrasted to $T_{1n}^{-1}=2\sigma w_1\propto H^{-2}T_{1e}^{-1}r^{-6}$ from Eq. (4). In order for Eqs. (25) and (26) to be valid, it is required that $b\ll R\ll L$ where $b=0.68(C/D)^{\frac{1}{3}}$ is the scattering length of one paramagnetic ion, $R=n_0^{-\frac{1}{3}}$ is the distance between paramagnetic ions, and $L=(DT_{1n})^{\frac{1}{2}}$ is the diffusion length during a relaxation time.[39]

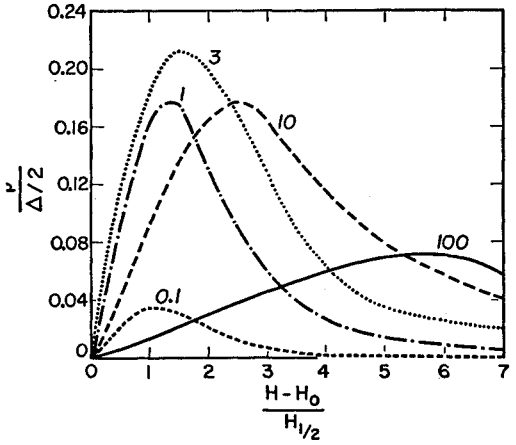

FIG. 5. Differential dynamic polarization calculated from Eq. (23) for a homogeneously broadened Lorentz line of half-width $H_{\frac{1}{2}}=H_0g_n/g$ for various values of the saturation parameter $s_0=(\gamma H_1)^2T_{1e}T_{2e}$.

Diffusion effects in dynamic nuclear polarization can be similarly treated.[40] In the special case that $f\ll 1$, i.e., if there is no bottleneck in the polarization process, then [see Eq. (17a)] the steady-state value $P\approx\Delta/2$ may be used in Eq. (12). Since α, β have the same dependence on r as does σ, we obtain

$$\begin{aligned}\partial p/\partial t=&-C\sum_k|\mathbf{r}-\mathbf{r}_k|^{-6}(p-p_0)-2w_1\varphi(p-p_0)\\&-2w_1\zeta p-F_-\sum_k|\mathbf{r}-\mathbf{r}_k|^{-6}(p-P_0)\\&-F_+\sum_k|\mathbf{r}-\mathbf{r}_k|^{-6}(p+P_0)+D\nabla^2 p, \quad (27)\end{aligned}$$

where $F_\pm=\frac{1}{2}\gamma H_1^2T_{1e}G(H-H_\pm)C$. If we let ζ become negligibly small, this equation can be written in the form of Eq. (24), and one finds for the space average polarization $\bar{p}$

$$\bar{p}(t)\approx\frac{P_0(F_--F_+)}{C+F_-+F_+}\cdot\frac{1-\exp[(-2\varphi w_1-\tau_{1n}^{-1})t]}{1+2\varphi w_1\tau_{1n}}, \quad (28a)$$

where

$$\tau_{1n}^{-1}=8.5n_0(C+F_-+F_+)^{\frac{1}{4}}D^{\frac{3}{4}}. \quad (28b)$$

We have assumed that $p(0)\approx p_0$ and that $W_2\propto F_1$ and $W_3\propto F_+$ are turned on at $t=0$. The validity conditions are now

$$[(C+F_-+F_+)/D]^{\frac{1}{4}}\ll n_0^{-\frac{1}{3}}\ll(D\tau_{1n})^{\frac{1}{2}}.$$

Equation (28a) displays a differential effect, but if we further assume that the lines are resolved so that we can take $F_-=0$, $F_+=\frac{1}{2}s_0C$, then the steady-state

[36] N. Bloembergen, S. Shapiro, P. L. Pershan, and J. O. Artman, Phys. Rev. 114, 445 (1959).
[37] G. R. Khutsishvili, Akad. Nauk Gruzin. SSR, Inst. Fiz. 4, 3 (1956).
[38] P. G. deGennes, J. Phys. Chem. Solids 7, 345 (1958).
[39] See, e.g., A. Abragam, *Principles of Nuclear Magnetism* (Oxford University Press, New York, 1961), Chap. IX.
[40] J. Winter, *Quantum Electronics* (Columbia University Press, New York, 1960), p. 184.

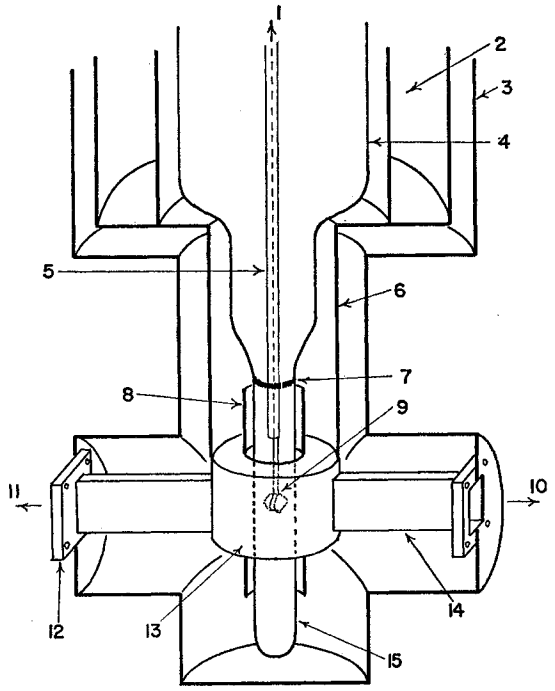

FIG. 6. Double-resonance cryostat, with thermal shields and vacuum jackets shown cut away. (1) Connected to nuclear resonance detector, (2) brass liquid nitrogen reservoir, (3) outer vacuum jacket, (4) silvered Pyrex liquid-helium container, (5) coaxial cable, (6) copper thermal shield, (7) Pyrex-to-quartz seal, (8) sleeve to reduce coupling of cavity through port holes, (9) rf coil and sample, (10) connected to klystron oscillator, (11) connected to microwave resonance detector, (12) mica vacuum window, (13) TE_{011} mode cavity, (14) thin-wall stainless steel waveguide 1 in.$\times\frac{1}{2}$ in., and (15) quartz tube.

polarization becomes

$$\bar{p}_{ss}\approx P_0\left(\frac{s_0}{2+s_0}\right)\frac{8.5n_0C^{\frac{1}{4}}D^{\frac{3}{4}}(1+\frac{1}{2}s_0)^{\frac{1}{4}}}{2\varphi w_1+8.5n_0C^{\frac{1}{4}}D^{\frac{3}{4}}(1+\frac{1}{2}s_0)^{\frac{1}{4}}}, \quad (29)$$

When $s_0\rightarrow\infty$, $\bar{p}_{ss}\rightarrow\Delta/2$ as in the simple model but the saturation behavior is different. The ratio of the characteristic polarization time to the relaxation time becomes $\tau_{0n}/T_{1n}\approx(1+\frac{1}{2}s_0)^{-\frac{1}{4}}$ if φw_1 is negligible. This is to be compared to $\tau_2/T_{1n}=(1+\frac{1}{2}s_0)^{-1}$ from Eq. (19c) in the similar case $f\ll 1$.

To summarize, diffusion theory provides an explanation for the unique nuclear relaxation time and polarization time usually observed and introduced *ad hoc* in the simple model of Sec. II A. Although the limiting values of the nuclear polarization are essentially the same in the two models, the diffusion-limited dynamic polarization rate is proportional to the $\frac{1}{4}$ root of the microwave power in Eq. (28b).

III. APPARATUS AND TECHNIQUES

We have constructed an apparatus to observe nuclear magnetic resonance simultaneously with paramagnetic resonance at helium temperatures. The details of the resonance cryostat are shown in Fig. 6. A cylindrical TE_{011} mode cavity resonant at $\nu_e\approx 9.4$ kMc/sec contains a quartz tube filled with liquid helium. The sample crystal is mounted in an rf coil so oriented that it does not couple with the cavity mode, as shown in Fig. 7. The coil is supported by a removable and rotatable rigid coaxial line connected to a nuclear resonance detector operated at $\nu_n\approx 17$ Mc/sec. The walls of the cavity are kept at 77°K by a thermal link to an N_2 reservoir, so that large microwave powers do not cause excessive boiling of helium. The crystal sample may be easily removed and a new one inserted with a negligible helium loss.

The cavity is coupled via a thin stainless steel waveguide to a standard transmission-type paramagnetic resonance spectrometer. From the cavity Q, etc., the H_1 field at the sample is estimated to be $H_1^2\approx 0.1\ P_c$, where H_1 is in oersteds and P_c is the average cavity power in watts. A Varian V-58 klystron is used to furnish up to $P_c=0.3$ w.

Paramagnetic resonance absorption was observed in the usual way by modulating the magnetic field and recording the derivative on a tape. For direct measurements of T_{1e}, a modified circuit, Fig. 8, was used to saturate the resonance by a high-power pulse (~20-w peak, 1-μsec duration) and then observe on a fast oscilloscope the recovery of the absorption signal.

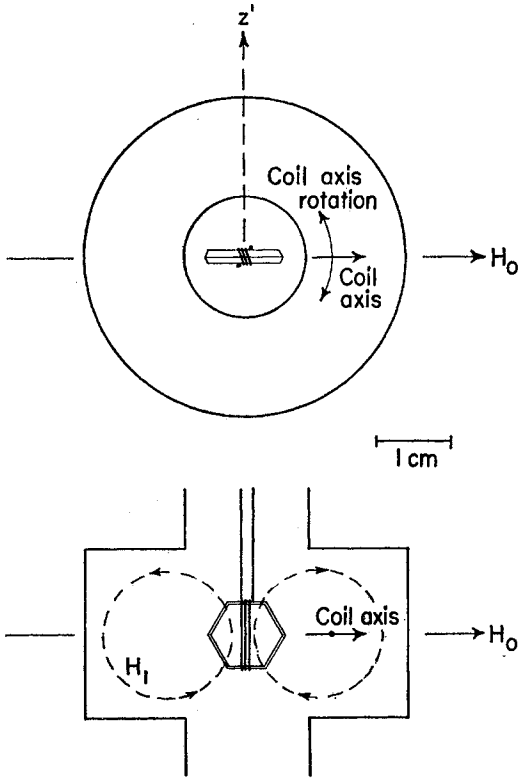

FIG. 7. Detail of cavity, H_1 flux lines, rf coil, crystal, and crystal axis z'.

One of the experimental difficulties is to observe the nuclear resonance absorption with a sufficiently small transition probability W_4 that the nuclear polarization is not perturbed; often $W_4<10^{-3}$ sec^{-1} is required. The resonance detector we have used is a modified[41] Pound-Knight[42] oscillator constructed by P. L. Scott. It operates stably over the range 2–20 Mc/sec at a minimum level of about 10 mv across the coil. To reduce W_4 still further, the coil was oriented so that only a small component of the H_{1n} field was perpendicular to H_0. The derivative of the nuclear resonance absorption was recorded on a tape using a modulation frequency of 280 cps.

The crystals of $(La,Ce)_2Mg_3(NO_3)_{12}\cdot 24H_2O$ were grown from aqueous solution in a desiccator at 0°C by seeding a saturated solution of a mixture of $Ce_2Mg_3(NO_3)_{12}$ and $La_2Mg_3(NO_3)_{12}$. The percentage of Ce was varied between 0.05% and 10% in the aqueous phase; the percentage in the crystals was not measured, but is presumably close to that of the solution. Perfectly clear crystals of ~150 mg could be grown in a day or so. The growth habit is a flat hexagonal plate, with the z' axis perpendicular to the plate.

Powder x-ray diffraction studies[43] of $Ce_2Zn_3(NO_3)_{12}\cdot 24H_2O$ indicate a rhombohedral unit cell with sides 13.1 A and interaxial angle 49°; see Fig. 9. There are two nonequivalent sites for the divalent ions, each surrounded by six water molecules. There is one site for the trivalent ion; the nearest hydrogen atom has been estimated to be 4.5 A away by magnetic resonance experiments.[44] One calculates on the basis of a simple cubic lattice from the density $\rho=1.99$ g/cm^3 that the average spacing is 3.0 A between protons and 8.5 A between La ions in the crystals we have used.

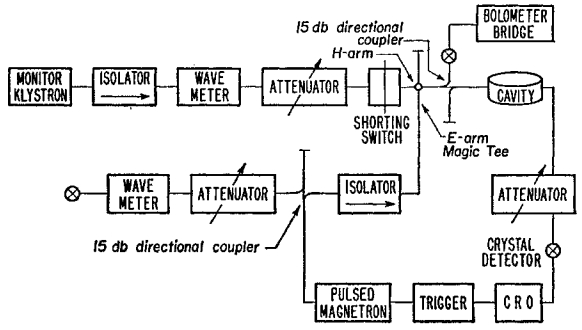

FIG. 8. Diagram of arrangement for measuring electron relaxation times.

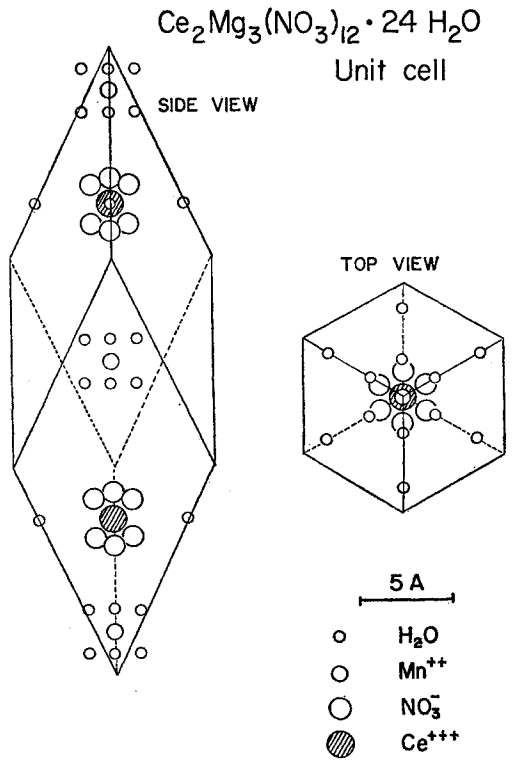

FIG. 9. Unit cell of double nitrate crystal.

IV. EXPERIMENTAL RESULTS AND INTERPRETATION

We have performed a fairly complete set of experiments on a number of single crystals of various Ce^{3+} concentrations. For a given crystal we observe: the Ce^{3+} paramagnetic resonance line, its shape, and the relaxation time T_{1e} between $1.7°K<T<2.7°K$; the proton magnetic resonance line, its shape, and the relaxation time T_{1n} in the temperature range $1.6°K<T<4.2°K$; the dynamic enhancement E of the proton polarization; the dependence of E on microwave power and field H; and the transient behavior of E. Sometimes we also observed ENDOR signals. These various experiments will be discussed separately below and correlated and compared to the theoretical expectations.

A. Paramagnetic Resonance of Ce^{3+} in $(Ce,La)_2Mg_3(NO_3)_{12}\cdot 24H_2O$

The resonance was first observed by Cook *et al.*,[45] and consists of a single line corresponding to the spin Hamiltonian

$$\mathcal{H}=g_{11}\beta H_{z'}S_{z'}+g_1\beta(H_{x'}S_{x'}+H_{y'}S_{y'}), \qquad (30)$$

with $g_{11}\leqq 0.03$, $g_1=1.83$. We suspended single crystals containing different Ce^{3+} concentrations in the cavity

[41] J. M. Mays, H. R. Moore, and R. G. Shulman, Rev. Sci. Instr. **29**, 300 (1958).

[42] R. V. Pound and W. D. Knight, Rev. Sci. Instr. **21**, 219 (1950).

[43] J. W. Culvahouse and R. C. Sapp (to be published); J. W. Culvahouse, W. Unruh, and R. C. Sapp, Tech. Rept. No. 2, November, 1960. Department of Physics and Astronomy, University of Kansas (unpublished).

[44] T. L. Estle, H. R. Hart, Jr., and J. C. Wheatley, Phys. Rev. **112**, 1576 (1958).

[45] A. H. Cooke, H. J. Duffus, and W. P. Wolf, Phil. Mag. **44**, 623 (1953).

TABLE I. Observed peak-to-peak width H_{pp} of the derivative of the paramagnetic resonance absorption of Ce^{3+} in $(La,Ce)_2Mg_3(NO_3)_{12}\cdot 24H_2O$; calculated half-width $H_{\frac{1}{2}}=\sqrt{3}H_{pp}/2$; calculated $T_{2e}=(\gamma H_{\frac{1}{2}})^{-1}$.

Cerium concentration (percent)	H_{pp} 4.2°K (oe)	H_{pp} 1.7°K (oe)	$H_{\frac{1}{2}}$ 1.7°K (oes)	T_{2e} 1.7°K (sec)
5	27	19	16.5	3.7×10^{-9}
1	7	7	6.0	1×10^{-8}
0.2	5	5	4.3	1.4×10^{-8}
0.05	5	5	4.3	1.4×10^{-8}

with the z' axis perpendicular to **H**. Measurements at 4.2°K and $H\approx3600$ oe yielded $g_\perp=1.830\pm0.003$ for 2% Ce; and $g_\perp=1.838\pm0.002$ for 100% Ce. The observed peak-to-peak separation, H_{pp}, of the derivative of the absorption is tabulated in Table I. The line shape for Ce concentrations $\sim1\%$ was approximately Lorentzian, so we calculate the half-width at half maximum $H_{\frac{1}{2}}=\sqrt{3}H_{pp}/2$, and also $T_{2e}=(\gamma H_{\frac{1}{2}})^{-1}$, where $\gamma=g_\perp\beta/\hbar=16.2\times10^6$ rad/oe. At the smallest concentrations, the linewidth may be attributed to the dipolar fields of the nuclei, chiefly protons in the water molecules. However, a 98% deuterated crystal did not exhibit an appreciably narrower line, so that anisotropy broadening is also a possibility. At concentrations greater than 1% there is clearly a Ce-Ce dipolar broadening.

Several small satellites located nonsymmetrically about the line center were observed, as shown in Fig. 10. Their intensity decreases both with decreasing temperature and decreasing Ce concentrations. Although we tentatively ascribe them to a dipolar interaction between pairs of Ce^{3+} ions, their nature is not really understood yet.

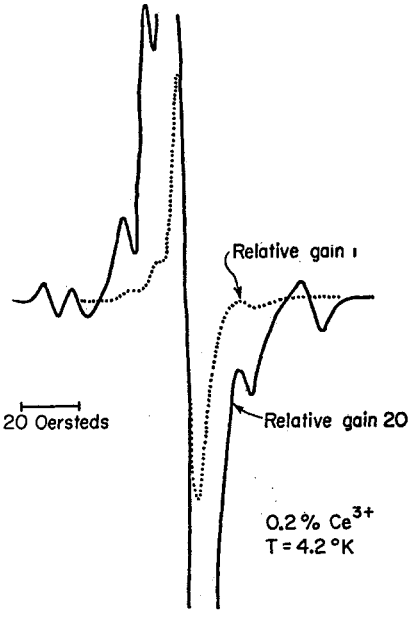

FIG. 10. Derivative of Ce^{3+} paramagnetic resonance absorption line in $(Ce,La)_2Mg_3(NO_3)_{12}\cdot24H_2O$, showing weak satellites.

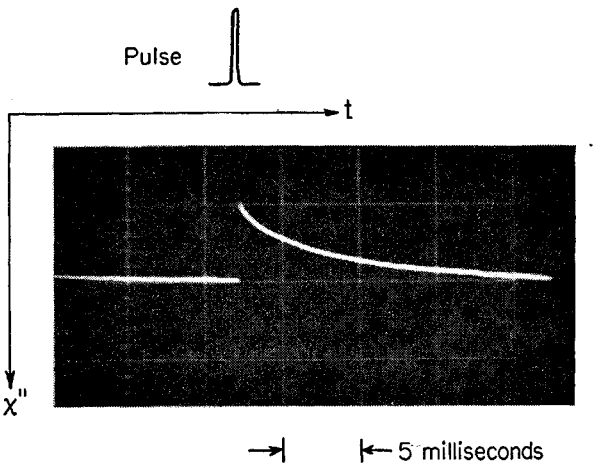

FIG. 11. Oscilloscope trace of recovery of Ce^{3+} absorption line following saturation by a pulse at $T=1.75°$ K for a 5% Ce crystal.

The forbidden transitions W_2 and W_3 were not distinctly observed. They would occur at fields $\pm g_nH_0/g\approx\pm6$ oe on either side of the main line center, whose minimum half-width was 4.3 oe. The satellite structure mentioned above perhaps masked them from observation.

To measure the relaxation time T_{1e} we applied high-power pulses to saturate the Ce^{3+} resonance, at the same time monitoring the absorption with a low power cw klystron, as in Fig. 8. After a pulse the cavity transmission decreases exponentially with a characteristic time T_{1e} to its unsaturated value if the crystal absorption is negligible compared to the cavity losses.[46] The pulse cavity power was $P_c\sim1$ w, corresponding to a saturation parameter $s_0>10^2$, while the monitor power was $P_c\sim10^{-5}$ w, corresponding to $s_0<10^{-2}$. Figure 11 is a photograph of an oscilloscope trace of the cavity transmission following a pulse. The traces were usually fairly exponential, indicating a unique relaxation time.

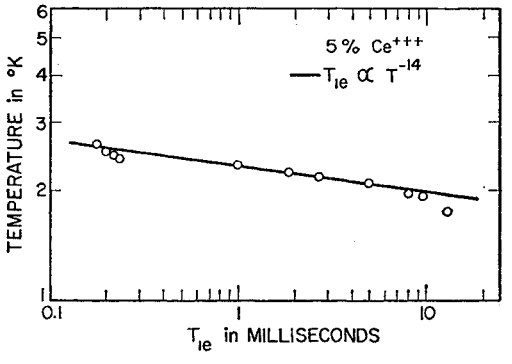

FIG. 12. Measured relaxation time T_{1e} of Ce^{3+} in $(Ce,La)_2Mg(NO_3)_{12}\cdot24H_2O$ as a function of temperature.

[46] K. D. Bowers and W. B. Mims, Phys. Rev. **115**, 285 (1959).

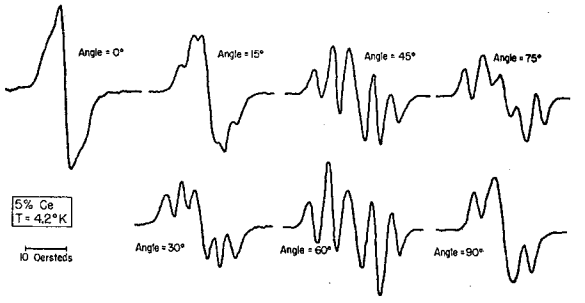

FIG. 13. Derivative of proton magnetic-resonance absorption at 4.2°K in $(Ce,La)_2Mg_3(NO_3)_{12}\cdot 24H_2O$ containing 5% Ce. The crystal was mounted as in Fig. 7 and rotated to various angles between z' and H_0.

Experiments were done in the temperature range $1.7°K<T<2.7°K$ for Ce concentrations of 0.05%, 0.2%, 1%, 5%, and 100%. Within an experimental error of about 20%, the relaxation time T_{1e} was found to be independent of concentration but extremely dependent on temperature, as shown in Fig. 12 for a 5% crystal. Down to 1.9°K the data fit very well the line $T_{1e}^{-1}\propto T^{14\pm 2}$, but for $T<1.8°K$ the increase of T_{1e} becomes less rapid.

This extremely rapid temperature variation of T_{1e} has also been observed by Finn *et al.*,[47] who explain it by a two-step phonon process from the ground state $M=\frac{1}{2}$ up to an excited state at energy $\mathcal{E}$, and back down to the ground state $M=-\frac{1}{2}$. The relaxation rate will be proportional to the Boltzmann population of the excited state: $T_{1e}^{-1}\propto \exp(-\mathcal{E}/kT)=\exp(-34/T)$. If our data of Fig. 12 are plotted $\log T_{1e}$ vs T^{-1}, they fit very well the straight line $T_{1e}^{-1}\propto \exp(-32\pm 2/T)$ and are thus in good agreement with Finn *et al.*

B. Nuclear Magnetic Resonance of Protons in $(Ce,La)_2Mg_3(NO_3)_{12}\cdot 24H_2O$

With the crystal mounted in the rf coil as in Fig. 7, we have measured the proton resonance line shape for various angles between z' and H_0. The results seem to be roughly independent of Ce concentration and temperature in the liquid-helium range. Figure 13 shows the absorption derivative at 4.2°K for a crystal containing 5% Ce. The structure is undoubtedly due to proton-proton dipolar interaction.[22] In Fig. 14 the data are summarized: The angular variation of the component lines is shown in comparison with curves of the form

$$H=H_0\pm\tfrac{3}{2}(g_n\beta/r^3)[3\cos^2(\theta-\varphi)-1].$$

A reasonable fit is obtained for the two curves shown ($\varphi=25°$ and 110°) for $r\approx 1.7$ A$\approx$the proton-proton spacing in H_2O. We have not analyzed the data in more detail since there are 24 H_2O molecules in a unit cell. The structure is probably explained solely by the term U_{ij} of Eq. (3). It has been shown[44] that the term A_{ik} in Eq. (2) is important in 100% Ce crystals at lower temperatures.

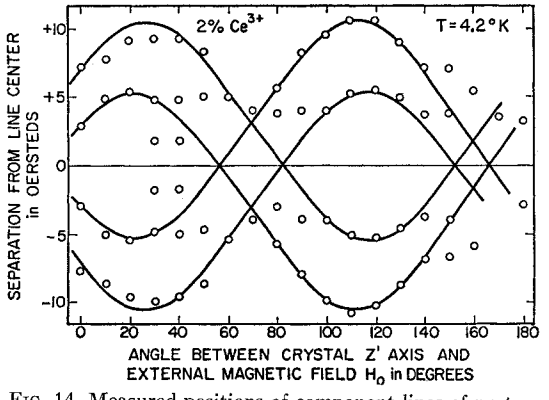

FIG. 14. Measured positions of component lines of proton magnetic-resonance in $(Ce,La)_2Mg_3(NO_3)_{12}\cdot 24H_2O$.

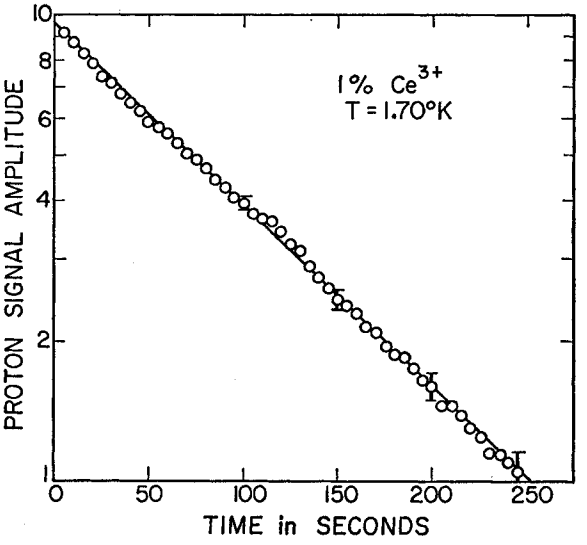

FIG. 15. Proton magnetic-resonance signal amplitude vs time following the switching off of the enhancing microwave power. The decay is quite exponential.

For the same crystals used in Sec. IV A we have measured the proton relaxation time T_{1n} by recording the transient decay of the nuclear resonance signal following the switching off of the microwave power used to enhance the polarization. The data were taken for several different rf levels of the Pound-Knight oscillator and the decay times were extrapolated to zero rf level in order to correct for a finite value of W_4; this correction was usually small, however. The data were taken with $z'\perp H_0$ and H_{1n} approximately parallel to H_0. It was always observed that the decay was exponential, corresponding to a unique relaxation time; this is illustrated in Fig. 15.

A summary of the results for various Ce concentrations and temperatures is given in Fig. 16. We note that (a) for all concentrations studied, the temperature dependence is given by $T_{1n}^{-1}\propto T^{7\pm 1}$; (b) at constant

[47] C. B. P. Finn, R. Orbach, and W. P. Wolf, Proc. Phys. Soc. (London) 77, 271 (1961); *Proceedings of the 7th International Conference on Low-Temperature Physics* (University of Toronto Press, Toronto, 1960), p. 43.

TABLE II. Comparison of the measured values of the proton relaxation time T_{1n} in $(Ce,La)_2Mg_3(NO_3)_{12}\cdot 24H_2O$ with the predictions of Eq. (26) and of Eq. (4).

Temperature (°K)	Cerium concentration (percent)	Observed T_{1n} (sec)	$(T_{1n})_{diff}$ (sec)	$(T_{1n})_{direct}$ (sec)
2.3	5	0.25	0.07	5
	1	9	0.37	26
	0.2	70	1.8	130
	0.05	80	7.4	520
2.1	5	0.48	0.1	18
	1	17	0.51	91
	0.2	130	2.5	450
	0.05	150	10	1800
1.9	5	1	0.14	68
	1	35	0.7	340
	0.2	270	3.5	1700
	0.05	300	14	6800

temperature the concentration dependence is roughly $T_{1n}^{-1}\propto n_0^2$ for Ce concentrations above 1%. Neither of these findings is in agreement with spin diffusion theory [Eq. (26)] which would predict $T_{1n}^{-1}\propto n_0T^{3.5}$ if we use the experimental result $T_{1e}^{-1}\propto T^{14}$ in the temperature region we are considering. We estimate the validity requirement for Eq. (26) by taking $D=3\times10^{-12}$ cm^2 sec^{-1}, $C=6.6\times10^{-48}T_{1e}^{-1}$, and $R=n_0^{-\frac{1}{3}}=(15\lambda\times10^{20})^{-\frac{1}{3}}$, where λ=fractional concentration of Ce. Then

$b\cong 0.08$ A,
$R=$ 23 A for $\lambda=0.05$
$=$ 107 A for $\lambda=0.0005$,
$L=$ 210 A for $\lambda=0.05$, $T=1.8$°K
$=$ 10 A for $\lambda=0.05$, $T=4.2$°K
$=3700$ A for $\lambda=0.0005$, $T=1.8$°K
$=$ 170 A for $\lambda=0.0005$, $T=4.2$°K.

Thus $b\ll R$ always, but the requirement $R\ll L$ is not satisfied at ~4°K where the diffusion range becomes too short.

We estimate the magnitude of T_{1n} from Eq. (26) to be $(T_{1n})_{diff}=(48\lambda)^{-1}T_{1e}^{\frac{1}{2}}$. This is evaluated from the T_{1e} measurements and compared to the data in Table II. The calculated values are shorter by an order of magnitude. Table II also shows for comparison estimates of T_{1n} based on a simple model in which $\langle T_{1n}^{-1}\rangle=2w_1\langle\sigma\rangle$, where $\langle\sigma\rangle$ is given by Eq. (4) averaged over all the nuclei within a "shell of influence" $r_0<r<r_1\lambda^{-\frac{1}{3}}$, where r_0=average minimum distance between Ce ion and proton, and $2r_1$=distance between La^{3+} ions. If we take $r_0=3$ A and $r_1=4$ A, this yields $(T_{1n})_{direct}=260\lambda^{-1}T_{1e}$; these values are tabulated in Table II and are an order of magnitude longer than the observed values of the proton relaxation time. Furthermore, this would give a distribution of relaxation times rather than a unique time as observed. Since the data indicate $T_{1n}\propto T_{1e}^{\frac{1}{2}}$, and the magnitude of T_{1n} is intermediate between $(T_{1n})_{diff}$ and $(T_{1n})_{direct}$, the over-all conclusion we reach is that the system at hand is an intermediate case between the direct simple model and the diffusion model.

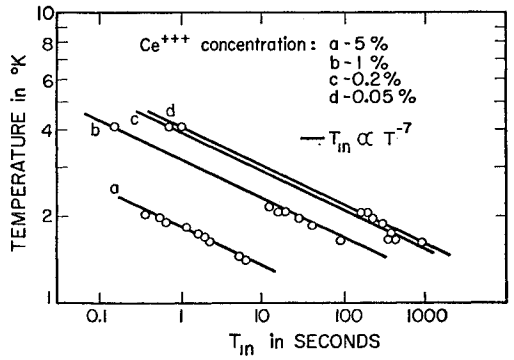

FIG. 16. Measured values of proton relaxation time T_{1n} in $(Ce,La)_2Mg_3(NO_3)_{12}\cdot 24H_2O$ for various Ce concentrations.

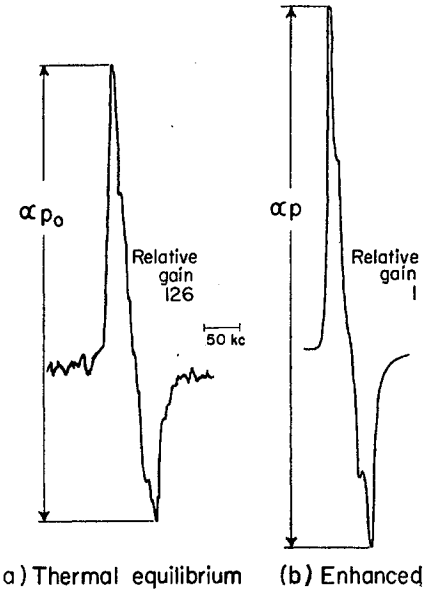

FIG. 17. (a) Proton resonance signal in a 1% Ce crystal at thermal equilibrium. (b) Proton resonance signal after saturation of forbidden transition W_3, showing a dynamic enhancement of the polarization, $E=p/p_0\approx 158$.

The concentration dependence $T_{1n}^{-1}\propto\lambda^2$ is difficult to understand. We note that the number of pairs of Ce^{3+} ions is proportional to λ^2 and that the probability to find a pair is appreciable for concentrations of a few percent. P. L. Scott has made some measurements of T_{1n} at the orientation $z'\|H_0$; his preliminary findings are $T_{1n}^{-1}\propto T^{12}$ and $T_{1n}^{-1}\propto\lambda^{1.3}$.

C. Dynamic Proton Polarization in $(Ce,La)_2Mg_3(NO_3)_{12}\cdot 24H_2O$

These experiments were performed on the same crystals for which T_{1n} and T_{1e} were measured above. The rf coil in Fig. 7 was made from one or two turns of 36 gauge copper wire to minimize the shielding of the crystal from the H_1 field. The procedure followed was

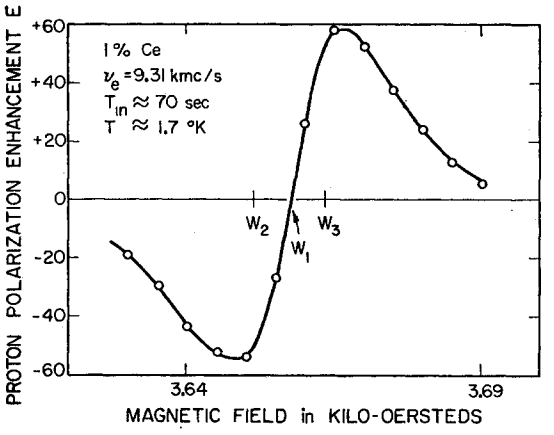

FIG. 18. Proton polarization enhancement E vs magnetic field H for a 1% Ce crystal.

to fix the klystron frequency ν_c to the cavity resonance and to set the field H at a series of values in the vicinity of $H_0(1\pm g_n/g)$. At each setting the proton resonance signal was measured by motor-tuning the Pound-Knight oscillator through the proton frequency ν_n. Only a small modulation field ($\approx$2 oe) was used and the derivative signal was recorded on a tape; since the operating conditions were held essentially constant, the amplitude of the signal was taken to be proportional to the nuclear polarization p. Sufficient time was allowed for the polarization to reach a steady state. The thermal equilibrium polarization p_0 was frequently measured by turning off the cavity power with a waveguide switch and waiting for a new steady state before recording the thermal equilibrium signal. Since the enhanced polarization p was 2 orders of magnitude larger than p_0, a calibrated attenuator in the signal amplifier was used to compare p and p_0. Figure 17 shows a typical recorded proton signal (a) at thermal equilibrium and (b) after saturating the microwave transition W_3; the enhancement $E=p/p_0\approx 158$.

Figure 18 shows the steady-state enhancement measured as a function of the field H for a 1% Ce crystal at 1.7°K and cavity power $P_c=300$ mw, the maximum available. The arrows indicate the (theoretical) positions of the fields for the W_1, W_2, and W_3 transitions. As expected, the enhancement has a maximum negative value near W_2, zero at W_1, and a maximum positive value near W_3. The spacing between the enhancement peaks is 16 oe, in comparison to a spacing between W_2 and W_3 of $2g_nH_0/g=12.1$ oe. The points of maximum slope of the absorption of the Ce^{3+} resonance for this crystal were separated by $H_{pp}=12$ oe, so that W_1, W_2, and W_3 would be partially resolved. The positive and negative enhancements were always observed to be equal in magnitude within experimental error. The enhancement at 4.2°K was small: $E\approx 2$.

Figure 19 shows a similar plot for a 5% crystal for which $H_{pp}\approx 33$ oe. The enhancement peaks are separated by 68 oe and this is clearly a case requiring the considerations of Sec. II B for unresolved lines. The enhancement curve E vs H does not have the shape of dG/dH as predicted by Eq. (22) for an inhomogeneously broadened line. In fact, there is good evidence that the Ce^{3+} lines are homogeneously broadened since we have never been able to "burn holes"[48] in them by saturation, even for very dilute crystals. The shape of the E vs H curve is explained in a qualitative way by Eq. (23) and Fig. 5; specifically, the position of the peak value of E far from the H_+ field is explained. Furthermore, other measurements for a series of cavity power levels indicate that the enhancement peak is moved farther away from H_0 as the power is increased, and that the enhancement at a given field increases to an optimum value and then decreases slightly for highest powers.

The maximum enhancement, $E=47$, in Fig. 19 is considerably less than the ideal value $E_i=605$; this discrepancy is not surprising in view of the poor resolution of W_1, W_2, and W_3. That the discrepancy is not due to insufficient power is indicated by Fig. 20. Half the maximum is achieved at a cavity power $P_c\approx 0.3$ mw, and the curve is apparently well saturated at 300 mw, where $s_0\gtrsim 10^2$. The data fit an expression of the form $E=E_{\max}(P_c/0.3)(1+P_c/0.3)^{-1}$, where P_c is the cavity power in milliwatts and $E_{\max}=47$. This saturation behavior is expected from Eq. (29) or Eq. (17b) if the extraneous relaxation φw_1 is negligible.

For the 1% Ce crystal, the saturation behavior was not of this form, but again the maximum enhancement, $E\approx 60$, was not limited by insufficient power. Since the forbidden transitions are partially resolved for this concentration, we attempt to explain the discrepancy from the ideal value by the simple model of Sec. II B and Eq. (17c): $E=E_i(1+f)^{-1}$. If we calculate f from Eq. (16b) using measured values of T_{1n} and T_{1e} and $n/N=2400$, we find $f\approx 0.5$, which is an order of magnitude too small to explain the discrepancy. At lower

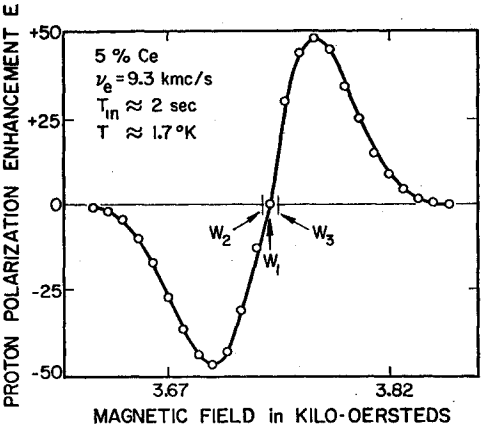

FIG. 19. Proton polarization enhancement E vs magnetic field H for a 5% Ce crystal.

[48] See, e.g., Fig. 2 in G. Feher, Phys. Rev. **114**, 1219 (1959).

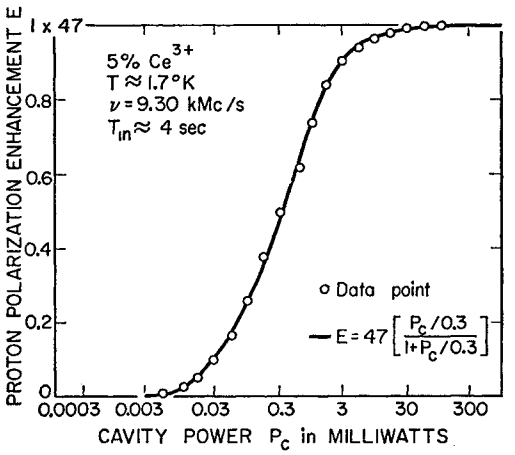

FIG. 20. Maximum enhancement E vs microwave cavity power.

concentrations and higher frequencies where the lines become better resolved, the enhancement may be limited by f, but in the cases reported here the limitation is mostly due to the overlap of W_1, W_2, and W_3.

In attempts to obtain the largest possible enhancement, measurements were made on a large number of crystals containing various Ce concentrations at a temperature of 1.7°K. The maximum observed enhancements were: $E=50$ for 5% Ce; $E=73$ for 2% Ce; $E=150$ for 1% Ce; $E=120$ for 0.2% Ce; and $E=90$ for 0.05% Ce. At 4.2°K the enhancements were small, $E\approx 3$, probably because T_{1e} is so short that $s_0 \ll 1$. Some crystals apparently were more perfect than others and had narrower Ce^{3+} resonance lines.

In summary, the largest enhancement observed at $\nu_e=9.3$ kMc/sec, $T=1.7$°K, and $H=3600$ oe was for a particularly well-grown crystal containing 1% Ce; the enhancement $E=150$ is a factor four less than the theoretical ideal and corresponds to an actual proton polarization of $p=3.2\%$ in a crystal weighing about 200 mg. Measurements[49] at $\nu_e\approx 34$ kMc/sec have yielded $E\approx 200$.

We have studied the transient build-up of the polarization and find that p exponentially approaches the steady-state value in a characteristic time τ_{0n} when the microwave power is turned on. When it is turned off, p decays exponentially in a time T_{1n}, and the measured ratio as a function of power is shown in Fig. 21 for a 1% Ce crystal at 1.7°K. From Eq. (28a) we expect that $\tau_{0n}/T_{1n}=(K+1)/[K+(1+\frac{1}{2}s_0)^{\frac{1}{2}}]$, where $K=2\varphi w_1/8.5n_0C^{\frac{1}{2}}D^{\frac{3}{2}}$. The data fit a curve of this form for $K\approx 2$.

A transient behavior of the electron polarization as suggested by Eq. (20b) has been observed: If the transition W_3 is strongly excited at $t=0$ corresponding to point a in Fig. 22, the electron resonance signal slowly increases to a value I_1 in a characteristic time τ_2 as the nuclei become polarized. Then if the polarization is quickly destroyed at b by an rf field H_{1n} at ν_n, the signal drops by an amount ΔI_1 [see Eq. (21)] and again slowly increases when this field is removed at c.

An ENDOR signal shown in Fig. 23 was observed by tuning the rf oscillator very slowly through ν_n. The signal shows no structure and has a width very comparable to the proton resonance line. Our interpretation is that the term A_{ik} in Eq. (2) is negligible in our experiments.

D. Dynamic Proton Polarization in $(Nd,La)_2Mg_3(NO_3)_{12}\cdot 24H_2O$

We have done a few experiments with crystals containing 1% Nd^{3+} enriched to 98.7% abundance in even-even isotopes. The paramagnetic resonance consists essentially of a single line with $g_1=2.72$. A satellite structure similar to Fig. 10 was again observed. The nominal linewidth is narrower than for Ce: $H_{pp}=3.8$ oe. The proton resonance lineshape was similar to that in Sec. IV B. No proper measurements of T_{1n} or T_{1e} were made, but we observed a proton polarization enhancement $E=31$ at 4.2°K and $E=19$ at 1.8°K. In contrast to Ce, the enhancement decreases at lower temperatures, probably for the reasons given in Sec. II A.

V. CONCLUSIONS

The actual physical system of electron spins and nuclear spins in a crystal is so complex that the simple theories of Sec. II cannot explain very well the details

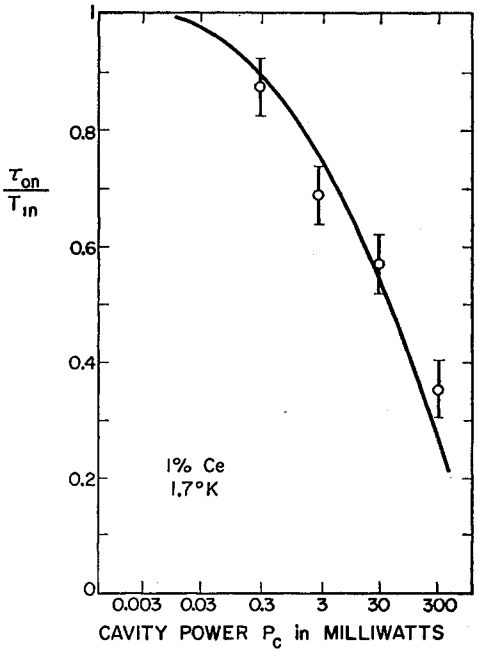

FIG. 21. Ratio of polarization time τ_{0n} to relaxation time T_{1n} vs microwave cavity power.

[49] M. Borghini and A. Abragam (private communication).

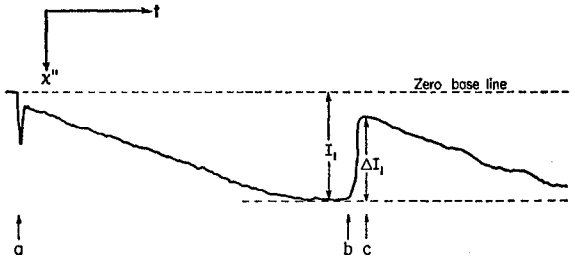

FIG. 22. Transient behavior of electron resonance signal $\propto \chi''$ in $(Ce,La)_2Mg_3(NO_3)_{12}\cdot 24H_2O$ containing 1% Ce at 1.46°K, for which $T_{1n}\approx 280$ sec. At time a the microwaves are turned on to induce the transition W_3; after a small instrumental transient, the signal builds up exponentially to a value I_1 with a time constant $\tau=190\pm 5$ sec. At b an oscillator at ν_n is turned on; at c it is turned off. The signal again builds up in a time constant $\tau\approx 180\pm 20$ sec.

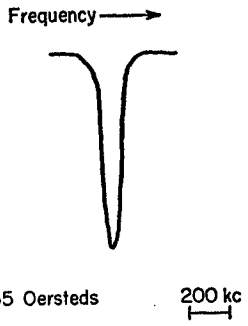

FIG. 23. Change in intensity (ENDOR signal) of Ce^{3+} resonance as rf oscillator is slowly tuned through proton resonance frequency ν_n.

of nuclear relaxation and dynamic polarization in the samples studied. The situation is complicated by spin diffusion, superposition of resonance lines, and unknown extraneous relaxation effects. However, a qualitative explanation of the principal features of the experiments can be given, and the actual polarizations obtainable are significant. For example, a target of protons polarized to about 25% for use in scattering experiments would appear to be a possibility at $\nu_e\approx 50$ kMc/sec and $T\approx 1.5$°K. A dynamic nuclear cooling[14] experiment closely related to Kittel's[50] proposal for metals would appear feasible. Consider, e.g., a very dilute $(Ce,La)_2Mg_3(NO_3)_{12}\cdot 24H_2O$ crystal in a microwave cavity cooled to 0.1°K and in a field $H_i\approx 10^4$ oe. If the forbidden transition W_3 is saturated the proton polarization may become as large as $p\approx 0.5$, corresponding to a spin temperature $T_i\approx 10^{-3}$ °K. The lattice vibrational energy will be negligible compared to the nuclear Zeeman energy. If the microwaves are turned off and the crystal is insulated, the temperature will fall to $T_f=H_fT_i/H_i$ if the field is reduced to H_f. For $H_f\sim 10$ oe, the temperature may become as low as $T_f\sim 10^{-6}$ °K. An experiment of this kind is in progress in our laboratory.

[50] C. Kittel, Physica 24, S88 (1958).

ACKNOWLEDGMENTS

We wish to acknowledge with much thanks the very considerable contributions of P. L. Scott in the design and construction of the apparatus, the performance of experiments, and discussions about their interpretation. Helpful discussions with R. A. Kamper, R. S. Anderson, and J. Winter are also gratefully acknowledged. H. J. Stapleton kindly observed the ENDOR signals of Fig. 23.

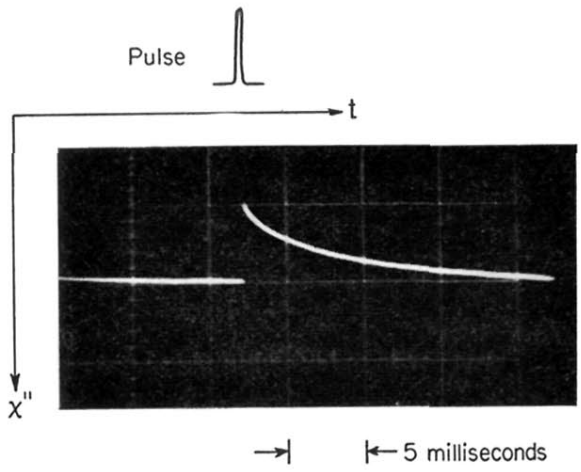

FIG. 11. Oscilloscope trace of recovery of Ce^{3+} absorption line following saturation by a pulse at $T=1.75°$ K for a 5% Ce crystal.